JOURNAL OF AIRCRAFT
Vol. 44, No. 6, November–December 2007

High Resolution Turbulence Treatment of F/A-18 Tail Buffet

Scott A. Morton,* Russell M. Cummings,† and Denis B. Kholodar‡
U.S. Air Force Academy, Colorado Springs, Colorado 80840

DOI: 10.2514/1.29577

Unsteady tail loads of the F/A-18 are computed using various turbulence models at an angle of attack consistent with buffet induced by leading-edge extension vortex breakdown. Comparison of these industry-standard Reynolds-averaged Navier–Stokes turbulence models with the detached-eddy simulation hybrid approach reveals the inadequacies of Reynolds-averaged Navier–Stokes methods and the ability of detached-eddy simulation to reproduce the observed unsteadiness at these conditions. Computed vortex breakdown position and frequencies of the detached-eddy simulation method are shown to be accurate by comparison to flight-test and experimental results. Finally, comparison of the detached-eddy simulation unsteady tail pressures with flight-test tail pressures reveal the ability of the method to accurately reproduce F/A-18 tail buffet loads and its readiness for inclusion in a fluid-structure interaction method.

I. Introduction

MANY of today's military vehicles exhibit vortex dominated flowfields. At a recent NATO Air Vehicle Technology conference, D. A. Lovell presented a review of "Military Vortices" [1], where he discussed the importance of understanding the phenomena for the success of current and future aircraft. He classified vortex flows into three categories: "those designed into a vehicle to improve performance, those which cannot be avoided and whose adverse affects must be minimized, and those that were not expected to occur" [1]. He gives examples of many of these vortex dominated flowfields: tip vortices on wings having low sweep, leading-edge extension vortices from the F-18 and F-16 aircraft, foreplanes on the Rafale, and flow over the MK-82 bomb, to name just a few. Because the aerospace industry often concentrates on cruise conditions for optimization of commercial aircraft, these vortical flowfields common in military aircraft are often not fully understood or able to be properly predicted. This is occurring at a time when the three largest U.S. fighter development programs (F/A-18E/F, F-22, and F-35) incorporate twin tail configurations and high angle-of-attack maneuvering.

The F-18 High Angle-of-Attack Research Vehicle (HARV; see Fig. 1) has proven to be an excellent source of data for researchers working on high angle-of-attack flowfields [2–4]. Extensive flight testing of the HARV has been conducted that provides a rich source of flow visualization, surface pressures, and aeroelastic information. The F/A-18 uses wing leading-edge extensions (LEX) to generate vortices which enhance the wing lift, and the twin vertical tails are canted to intercept the strong vortex field and increase maneuverability. At large incidence, the LEX vortices break down upstream of the vertical tails, resulting in a loss of yaw control power and severe aeroelastic effects [5]. The ultimate goal of computationally modeling the flowfield shown in Fig. 1 would be to accurately simulate the aeroelastic impact of the LEX vortices on the twin vertical tails. Previous predictions of the HARV flowfield include Reynolds-averaged Navier–Stokes (RANS) computations with solid tails [6], detached-eddy simulation (DES) predictions showing the impact of the breakdown region on the vertical tails [7], and fully aeroelastic tails with laminar off-body flow and flow control methods for alleviating tail buffet [8]. The current level of simulation technology, however, has not allowed for accurate prediction of vortex breakdown, and the unsteady flow downstream of breakdown, at flight Reynolds numbers. Because of this, researchers have spent time computing flows over simpler geometries, such as slender forebodies and delta wings, to improve their simulation capabilities. However, the advent of hybrid turbulence models may finally allow for the accurate prediction of full aircraft flowfields at high incidence.

Although advances have taken place in areas such as grid generation and fast algorithms for solutions of systems of equations, computational fluid dynamics (CFD) has remained limited as a reliable tool for prediction of inherently unsteady flows at flight Reynolds numbers. Current engineering approaches to prediction of unsteady flows are based on solution of the Reynolds-averaged Navier–Stokes equations. The turbulence models employed in RANS methods necessarily model the entire spectrum of turbulent motions. Although often adequate in steady flows with no regions of reversed flow, or possibly exhibiting shallow separation, it appears inevitable that RANS turbulence models are unable to accurately predict flows characterized by massive separation. Unsteady, massively separated flows are characterized by geometry-dependent and three-dimensional turbulent eddies. These eddies, arguably, are what defeat RANS turbulence models from predicting flows of any complexity.

To overcome the deficiencies of RANS models for predicting massively separated flows, Spalart and Allmaras [9,10] proposed detached-eddy simulation with the objective of developing a numerically feasible and accurate approach combining the most favorable elements of RANS models and large-eddy simulation (LES). The primary advantage of DES is that it can be applied at high Reynolds numbers, as can Reynolds-averaged techniques, but DES also resolves geometry-dependent, unsteady three-dimensional turbulent motions as in LES. The unstructured finite volume solver Cobalt [11] has been used in conjunction with DES successfully on a number of complex problems, including a supersonic base flow [12], delta wing vortex breakdown [13], a square with rounded corners [14], the F-15E at high angle of attack [15], and the F/A-18E with unsteady shock buffet [16].

The specific aim of this work is to document the effects of applying detached-eddy simulations to the F/A-18C at a condition consistent with vortex breakdown. Computations are made for the F/A-18C at $\alpha = 30$ deg, $M_\infty = 0.2755$, and $Re_{\bar{c}} = 13 \cdot 10^6$, which determines the importance of turbulence model choice and the importance of

Presented as Paper 1676 at the 45th AIAA/ASME/ASCE/AHS/ASC Structures, Structural Dynamics & Materials Conference, Palm Springs, California, 19–22 April 2004; received 3 January 2007; revision received 11 April 2007; accepted for publication 13 April 2007.

*Professor of Aeronautics; currently U.S. Air Force Seek Eagle Office. AIAA Associate Fellow.
†Professor of Aeronautics. AIAA Associate Fellow.
‡Research Engineer; currently Bombardier. AIAA Member.

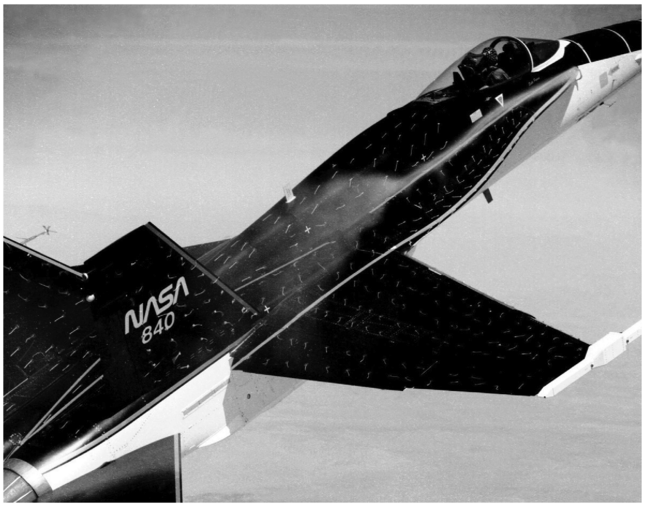

Fig. 1 NASA F-18 High Angle-of-Attack Research Vehicle (HARV). (Photo Courtesy of NASA Dryden.)

using highly refined grids (including automatic mesh refinement) on the accurate prediction of complex vortical flowfields. Comparisons are made between two industry-standard unsteady Reynolds-averaged Navier–Stokes (U-RANS) methods, and the Spalart–Allmaras DES (SADES) method. The resulting predictions are compared with available flight-test data for the F-18 HARV. Of this list, only SADES accurately predicts the postbreakdown flowfield, and therefore is capable of modeling tail buffet on the F/A-18C.

II. Numerical Method

In this section, a brief description of the numerical method is provided. Full details of the computational scheme and the solution method are presented in [11]. The configuration of interest is the F/A-18C with leading-edge flaps set to −33 deg and trailing edge flaps set to 0°, and the diverter slot with flow through the LEX is closed. This configuration closely matches the F-18 HARV for the chosen flight conditions.

Solutions were computed with the commercial version of Cobalt developed by Cobalt Solutions [11]. Cobalt solves the unsteady, three-dimensional, compressible Navier–Stokes equations on a hybrid unstructured grid. The code has several choices of turbulence models, including Spalart–Almaras (SA), and Menter's shear stress transport (SST) RANS, as well as DES versions of SA and SST. All simulations were computed on unstructured meshes with prisms in the boundary layer and tetrahedra elsewhere on half-span surface geometries. The computational meshes were generated with the software packages GridTool [17] and VGRIDns [18].

A. Turbulence Models

For simulation of turbulent flows, the governing equations are suitably averaged, yielding turbulent stresses that require a model. A Boussinesq approximation is invoked in the momentum equations and the turbulent eddy viscosity μ_t is used to relate the stresses to the strain rate. The turbulent heat flux is also modeled using a gradient-transport hypothesis, requiring specification of a turbulent thermal conductivity k_t. The Reynolds analogy is applied and the turbulent heat flux is modeled using a constant turbulent Prandtl number of 0.9. Using turbulent eddy viscosity and turbulent conductivity, the variable μ is replaced with $(\mu + \mu_t)$ and k is replaced with $(k + k_t)$ in the governing equations.

B. Menter's Shear Stress Transport Model

Menter's shear stress transport model [19] is a hybrid k–ε and k–ω turbulence model. Typical k–ω models are well behaved in the near wall region where low Reynolds number corrections are not required. However, they are generally sensitive to the freestream values of ω. On the other hand, k–ε models are relatively insensitive to freestream values, but behave poorly in the near wall region. Menter proposed a hybrid model. The SST model uses a parameter to switch from k–ω to k–ε in the wake region to prevent the model from being sensitive to freestream conditions.

C. Spalart–Allmaras Turbulence Model

The Spalart–Allmaras [9] one-equation model solves a single partial differential equation for a working variable $\tilde{\nu}$ which is related to the turbulent viscosity. The differential equation is derived by "using empiricism and arguments of dimensional analysis, Galilean invariance and selected dependence on the molecular viscosity" [9]. The model includes a wall destruction term that reduces the turbulent viscosity in the laminar sublayer. The turbulent viscosity is obtained from the turbulent kinematic viscosity by $\mu_t = \rho\nu_t$.

D. Detached-Eddy Simulation

Detached-eddy simulation was proposed by Spalart et al. [20]. The motivation for this approach was to combine large-eddy simulation with the best features of Reynolds-averaged Navier–Stokes methods. RANS methods have demonstrated an ability to predict attached flows very well with a relatively low computational cost. LES methods have demonstrated an ability to compute separated flowfields accurately, but at a tremendous cost for configurations with boundary layers. Spalart's DES method is a hybrid of LES and RANS, which combines the strengths of both methods.

The DES model was originally based on the Spalart–Allmaras one equation RANS turbulence model (detailed in Sec. II.C). The wall destruction term presented in the aforementioned section is proportional to $(\tilde{\nu}/d)^2$, where d is the distance to the wall. When this term is balanced with the production term, the eddy viscosity becomes proportional to $\hat{S}d^2$ where $\hat{S}$ is the local strain rate. The Smagorinski LES model varies its subgrid scale (SGS) turbulent viscosity with the local strain rate, and the grid spacing: $\nu_{\mathrm{SGS}} \propto \hat{S}\Delta^2$, where $\Delta = \max(\Delta x, \Delta y, \Delta z)$. If d is replaced with Δ in the wall destruction term, the SA model will act as a Smagorinski LES model.

To exhibit both RANS and LES behavior, d in the SA model is replaced with

$$\tilde{d} = \min(d, C_{\mathrm{DES}}\Delta)$$

When $d \ll \Delta$, the model acts in a RANS mode and when $d \gg \Delta$, the model acts in a Smagorinski LES mode. Therefore, the model switches into LES mode when the grid is locally refined.

DES was implemented in an unstructured-grid method by Forsythe et al. [21]. They determined the C_{DES} constant should be 0.65, consistent with the structured grid implementation of Spalart et al. [20] when the grid spacing Δ was taken to be the longest distance between the cell center and all of the neighboring cell centers.

A Newton subiteration method is used in the solution of the system of equations to improve time accuracy of the point-implicit method and approximate Jacobians. In the calculations presented next, a typical number of three Newton subiterations is used for all time-accurate cases.

E. Grid Generation and Solution Method

Spalart [10] described the process of grid design and assessment for DES, defining important regions of the solution and offering guidelines for grid densities within each region. The "Young-Person's Guide" [10] (YPG) forms a basis for interpretation of many of the results presented next. One of the traditional motivations for using unstructured grids has been the ability to rapidly create grids around complex geometries. There are other positive attributes of unstructured grids that are relevant to DES. Most notably, it is possible to concentrate points in the region of interest (i.e., the vortex core or aft of breakdown) and rapidly coarsen the grid away from these areas. This region of interest was termed the "focus region" in the YPG. Another advantage exploited in the present study is the

isotropic cells generated in the LES region by most unstructured-grid generation packages. The YPG reference describes the desirability of having isotropic grid cells in the focus region in which unsteady, time-dependent features are resolved. For this reason, unstructured grids are good candidates for use in DES because near isotropy of the grid cells in the LES region is assured by most grid generation packages.

Morton et al. [22] applied the YPG guidelines to three massively separated flows of interest: forebody in a crossflow, flow over a delta wing at moderate angle of attack, and the flow over an F-15E at high angle of attack. In the latter two cases, an extensive grid sensitivity study was performed by systematically varying the grid by a scale parameter allowing a very consistent analysis of grid effects when using the DES method of computing massively separated flows. A further refinement of the delta wing grids was presented in [23] as well as the first use of adaptive mesh refinement with DES.

Another important grid technology that is particularly well suited for DES is adaptive mesh refinement. Pirzadeh [24] presented a method based on a tetrahedral unstructured-grid technology developed at NASA Langley Research Center with application to two configurations with vortex dominated flowfields. The large improvement of the adapted solutions in capturing vortex flow structures over the conventional unadapted results was demonstrated by comparisons with wind-tunnel data. Pirzadeh showed the numerical prediction of these vortical flows was highly sensitive to the local grid resolution and he also stated that grid adaptation is essential to the application of CFD to these complicated flowfields. His most successful computations were performed using an inviscid method due to the inadequacies of standard turbulence models in computing these complicated flowfields. Pirzadeh's method is applied to the F/A-18C in the current study. A mean flow solution on a baseline grid is used to create an adaptively refined mesh and the new grid is used with DES to compute the unsteady flowfield for these two configurations. All meshes of the current study produced average y^+ values less than one.

The proposed method for simulating aircraft at flight Reynolds numbers in conditions of massively separated flow is as follows:

1) Use a time-accurate unstructured-grid solver to allow rapid turnaround of grids on complex configurations; the solution must have at least second-order spatial and temporal accuracy.

2) Use DES as the underlying turbulence treatment to obtain accurate unsteady loads and mean quantities; this requires a low dissipation solver.

3) Use adaptive mesh refinement (AMR) to improve the grid resolution in critical areas with nonlinear flowfield phenomena.

Following this method has been shown to accurately predict vortex flowfields with vortex breakdown [7].

III. Results

This section presents results of the numerical simulations for the F/A-18C with comparison to the NASA HARV flight-test data. The results section will be separated into subsections for comparison of solutions with various turbulence models and then comparison of SADES solutions with flight-test data.

All F/A-18C cases were run at 30 deg angle of attack, a Mach number of 0.2755, and a standard day altitude of 20,000 ft. The resulting Reynold's number was 13 million based on the mean aerodynamic chord of the aircraft (12 ft). The baseline grid of 3.6 million cells was generated with VGRIDns after starting from a geometry file provided by Cobalt Solutions LLC from their F/A-18C work. Unsteady SADES turbulence model simulations were performed using the baseline grid. A time-averaged SADES solution was used to produce an AMR grid with 3.9 million cells by following the approach outlined in [7]. All time-accurate simulations were run for over 10,000 iterations with second-order temporal and spatial accuracy, three Newton subiterations, and a time step of 0.0005 sec. The chosen time step results in a time step nondimensionalized by the freestream velocity and mean aerodynamic chord of 0.0012. This characteristic time step was found adequate in previous studies of vortex breakdown and massively separated flows [7,15,25].

Figure 2a depicts a top view of the surface mesh and Fig. 2b depicts a cross-plane at a station 450 in. aft of the origin for both the baseline grid and the AMR grid. The AMR grid has enhanced resolution in the core of the LEX vortex and over the wing. These enhanced grid regions are due to the AMR based on a vorticity isosurface corresponding to separation regions at these locations and due to the vorticity in the LEX vortex core.

A. Vortical Flow Prediction Ability of Turbulence Models

Solutions were computed using the SST, SA, and SADES turbulence models to determine their effect on the flowfield. Solutions for all three methods were computed using the same grid, time step, and number of subiterations to provide a consistent comparison. Figures 3a–3c depict snapshots of solutions for each method with the surface colored by pressure and an isosurface of vorticity shown. The chosen vorticity level for the isosurface and the pressure color map are held fixed. Although the snapshots are not necessarily synchronized in time, the overall differences are striking. The SADES solution (Fig. 3c) produces a much more detailed view

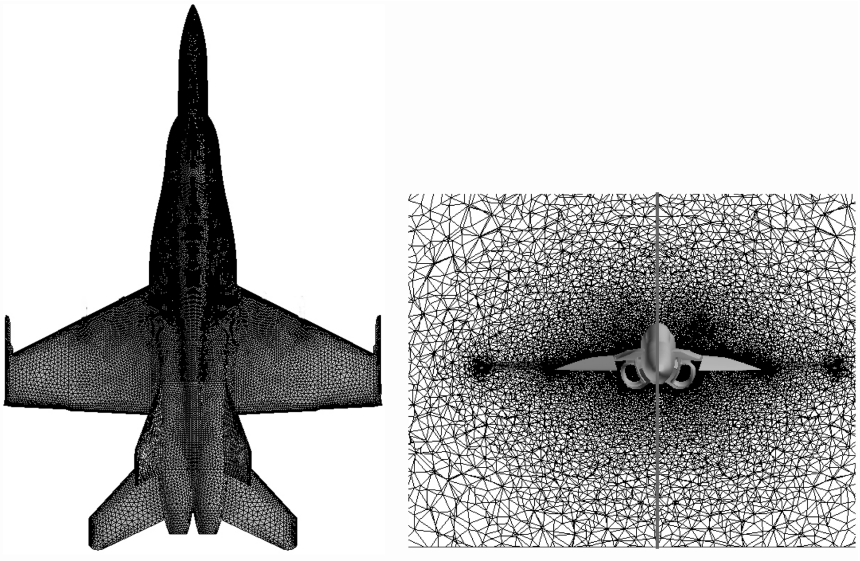

a) b)

Fig. 2 Baseline grid: a) top view of 3.9 million cells, b) 3.6 million cells (left) and AMR grid of 3.9 million cells (right). Darkened regions above the LEX show adapted mesh refinement of the vortex.

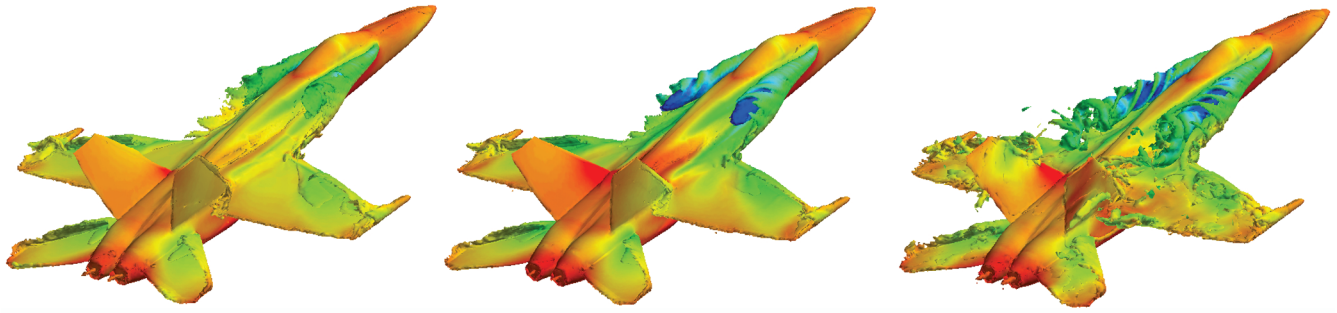

a) SST b) SA c) SADES

Fig. 3 Isometric views of the F/A-18C at $\alpha = 30$ deg, $Re_c = 13 \times 10^6$, leading-edge flaps set to −33 deg, trailing-edge flaps set to 0 deg, with no diverter slot present.

of the simulation because it is able to capture much finer flowfield scales. The SST (Fig. 3a) and SA (Fig. 3b) models are unable to capture the proper postbreakdown behavior or the leading-edge separation regions of the wing, horizontal, and vertical tails. It is also apparent that the SST LEX vortex pressure footprint on the surface is significantly different than either the SA or SADES solutions. The low-pressure region represented by a dark green color is greatly reduced in size on the SST solution. The SADES solution is also capturing the vortical substructures around the primary vortex.

A common definition of vortex breakdown is the location where the streamwise velocity component is zero in the core. The coordinates of this point along the core were tracked in time for each of the methods (SST, SA, and SADES). Figure 4 depicts the time histories of the three methods as well as the flight-test and experiment maximum and minimum mean values of vortex breakdown presented in [26]. Three things are obvious from Fig. 4. First, the amplitude of oscillation for the SST and SA models is almost negligible compared with the SADES simulation. Second, the SST solution predicts breakdown far upstream of the flight-test or experimental values, whereas the SA solution predicts the breakdown location downstream of the flight-test and experimental results. Third, the SADES solution gives a mean value of vortex breakdown location well within the flight-test and experimental data. It should also be noted that the computed nondimensional primary frequency of the breakdown oscillation is 0.2 in the range of frequencies commonly found in the literature [27] for vortex breakdown. This inability of commonly used turbulence models to accurately compute a solution with breakdown is well documented in the literature and is due to the large amount of eddy viscosity these

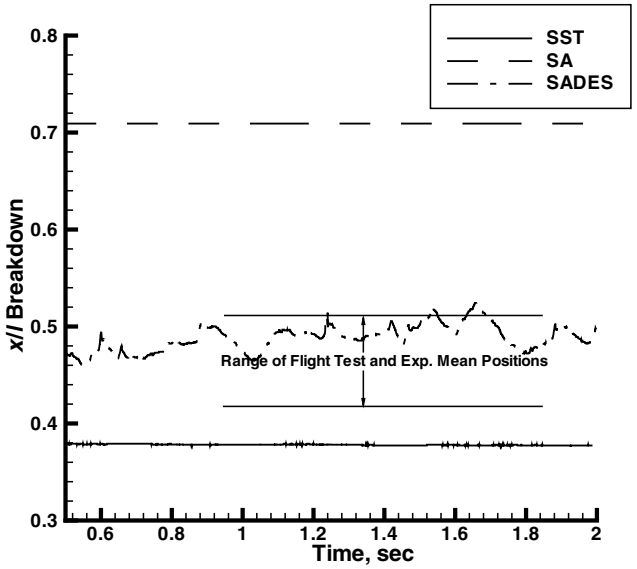

Fig. 4 Time histories of the streamwise coordinate of vortex breakdown referenced to the vehicle nose ($x = 0$) and scaled by the vehicle length l for the SST, SA, and SADES methods.

models put into the core of vortices [13]. Several researchers have proposed alterations to the RANS turbulence models by incorporating some form of a rotation correction for the flow in vortical regions. The disadvantage of this approach is the fact that the simulation will still be operating in a RANS mode and give solutions that are relatively steady postbreakdown as opposed to an LES approach that resolves the eddies that produce the unsteadiness. It is clear in Figs. 3 and 4 that the SADES method does not suffer from the same problem as the RANS methods due to the fact that eddy viscosity is computed based on subgrid scale turbulence, automatically minimizing the amount of spurious eddy viscosity that is placed in the core of vortices.

Figure 5 is a well-known plot in the literature of the streamwise location of the LEX vortex breakdown as a function of angle of attack [26]. The current solutions fall in the range of flight tests and experiments plotted at 30 deg angle of attack. The previous comparisons of the method with the flight-test and experimental data was poor due to the incorrect flap settings and the diverter slot being uncovered [7].

The effect of the various turbulence methods on computing the loads for these massively separated flows is demonstrated in Figs. 6a and 6b. Figure 6a shows the lift force on the vehicle as a function of time for the SST, SA, and SADES methods. As in the case of vortex breakdown position, the lift force computed with SADES has a significant amount of frequency content when compared with SST or SA. Also, the effect of the SST method predicting vortex breakdown far upstream is seen in a loss of lift. Figure 6b shows similar trends in the drag force. The interesting feature to note in Fig. 6b is the large amplitude of oscillation in drag force computed with the SA model.

To determine the effect of using different turbulence models on the computed solutions frequency content, data was obtained at a "virtual" pressure port on the inboard and outboard sides of the vertical tail at 10% back from the leading edge and at 85% of the span. A power spectrum density (PSD) analysis was performed using MATLAB on the data from these pressure ports and presented in Fig. 7, with the inboard port numbered 25 and the outboard port numbered 26 (matching the flight-test numbering system). The frequency output of the PSD was scaled by the mean aerodynamic chord and freestream velocity to produce the nondimensional Strouhal frequency. The power was scaled by the number of points in the time history. Because the number of points and the time step were consistent between the three methods, the magnitude of the power from one method relative to another method becomes significant. All three of the methods show a peak Strouhal frequency of approximately 0.5. The SADES method shows a three-orders-of-magnitude increase in the power for the majority of the frequencies up to a Strouhal number of three. Also, the typically seen $-5/3$ slope roll off in power is at a much lower frequency in the SST and SA simulations than the SADES simulations. This shows the ability of the SADES method to resolve a greater frequency spectrum.

B. Comparison to NASA F-18 HARV Flight-Test Data

This section presents comparison of the computed SADES solutions with F-18 HARV flight-test data from NASA Dryden

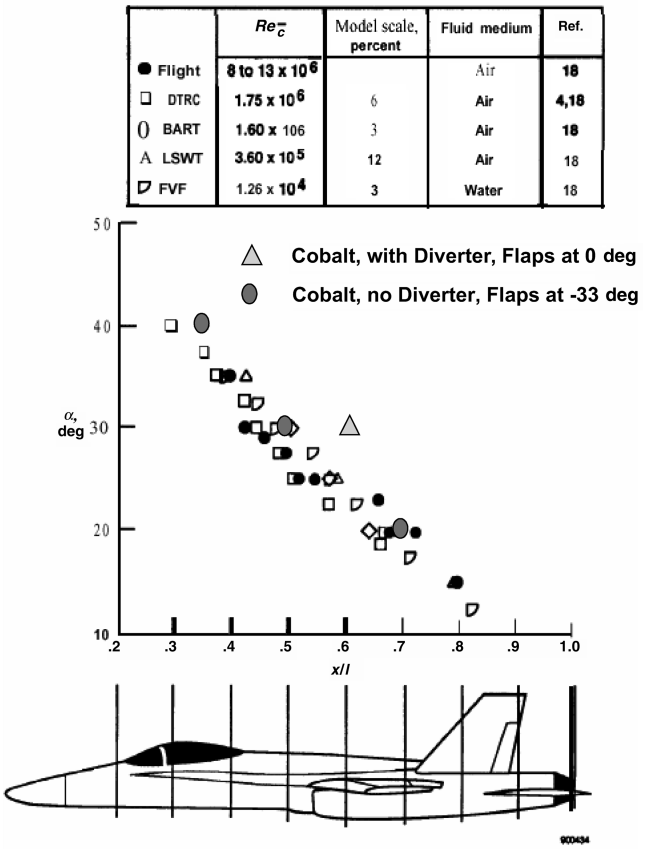

Fig. 5 Streamwise LEX vortex breakdown position as a function of angle of attack, extracted from [26]; SADES mean vortex breakdown position marked with filled oval symbols.

Flight Research Center [4]. The HARV was instrumented with 32 Kulite pressure sensors, half on the inboard and half on the outboard sections of the right vertical tail (see Fig. 8) [26]. The Kulite pressures were stored every 30 ms as a function of time. The available pressures were stored relative to a reference pressure that is unfortunately unknown. The lack of known reference pressures allowed only frequency comparisons rather than frequency and amplitude comparisons of the SADES data with flight-test data. The circled pressure ports of Fig. 8 are those used for comparison with the SADES simulations.

The flight-test and SADES simulation port pressures were analyzed with MATLAB's PSD function as discussed in an earlier section. Because the flight-test data have a different time step and period of time (40 sec), the power resulting from a PSD analysis will not be a one-to-one match but the frequencies and characteristic shapes of the PSD should match. All 32 pressure ports were analyzed but only a representative set are shown. The ports chosen for presentation provide a series of data along the leading edge and a variation in span, as well as a series of chord locations at a particular span. Figures 9a–9c depict the comparison of SADES and flight-test data. Figure 9a shows the PSD data for flight-test and SADES simulation for ports 1 and 2, Fig. 9b shows ports 13 and 14, Fig. 9c shows ports 17 and 18, and Fig. 9d shows ports 25 and 26. In all cases, the frequency content shows quite good comparison between the flight-test and SADES simulations. All of the ports show a wide peak amplitude range corresponding to Strouhal numbers between 0.45 and 0.8 for both flight-test and SADES simulations. This frequency range corresponds to pressure sweeps over the tail surface observed in a movie clip of the SADES simulation. Unfortunately, the published first bending mode is at a Strouhal number of approximately 0.66, explaining why the tail is so aeroelastically active at this flight condition. Most of the ports also show matches in slopes of the PSD for the Strouhal range of 1–10. Ports 1 and 2 compare least favorably in the higher Strouhal range (1–10). These ports are located in a region of very complicated flow structures (as seen in Fig. 3c). An increase in grid resolution in this area is probably warranted. It is also interesting to note that when the flight-test curves for each port lie on top of each other, this is true for the SADES solutions as well (Figs. 9c and 9d), and when the flight-test curves are separated, they are separated by approximately the same amount in the SADES solutions (Fig. 9b). A consistency is noted in the level of power between inboard and outboard ports for both flight test and SADES, i.e., when the inboard port has a higher power for flight test that is true as well for the SADES simulation. Finally, when the curves cross, this occurs at approximately the same frequency for flight test and SADES (Fig. 9d). The overall comparison of frequency content is remarkably good for the SADES solutions, demonstrating the utility of the method for tail buffet computations at flight Reynolds numbers.

IV. Conclusions and Recommendations

The combined SADES and AMR grid approach was used to compute solutions of the F/A-18C in a configuration closely matching the F-18 HARV flight-test vehicle. The SST and SA turbulence methods were shown to be inconsistent with each other

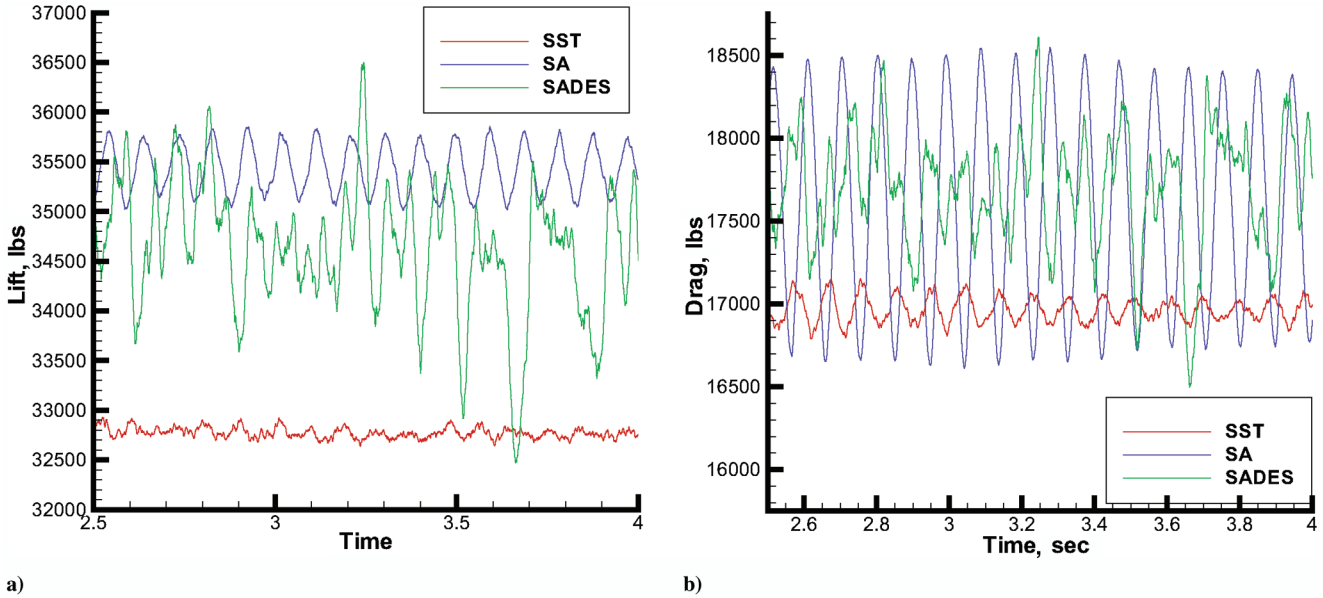

Fig. 6 Time histories of the a) lift force and b) drag force in pounds for the SST, SA, and SADES methods.

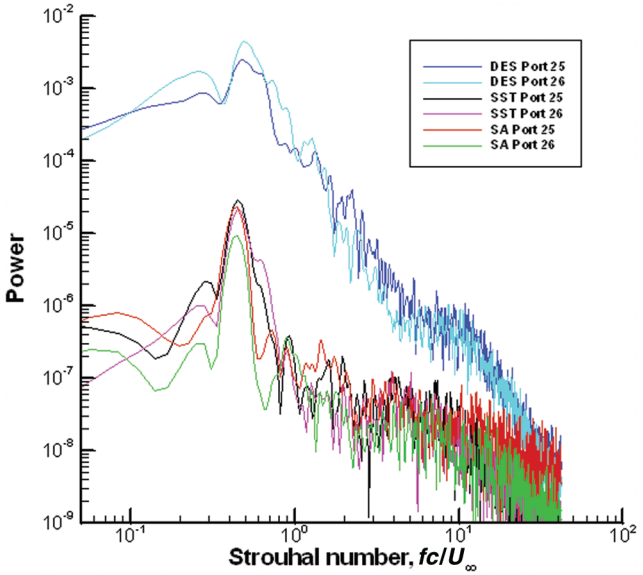

Fig. 7 Power spectrum density comparison for SST, SA, and SADES turbulence models.

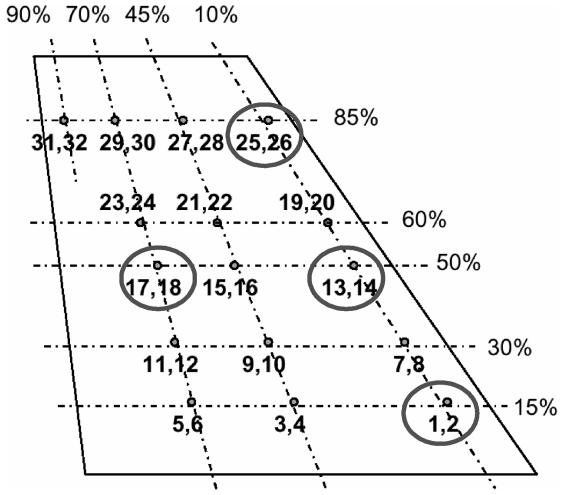

Fig. 8 F-18 HARV Kulite pressure sensors on right vertical tail [26]. Odd port numbers are inboard and even are outboard.

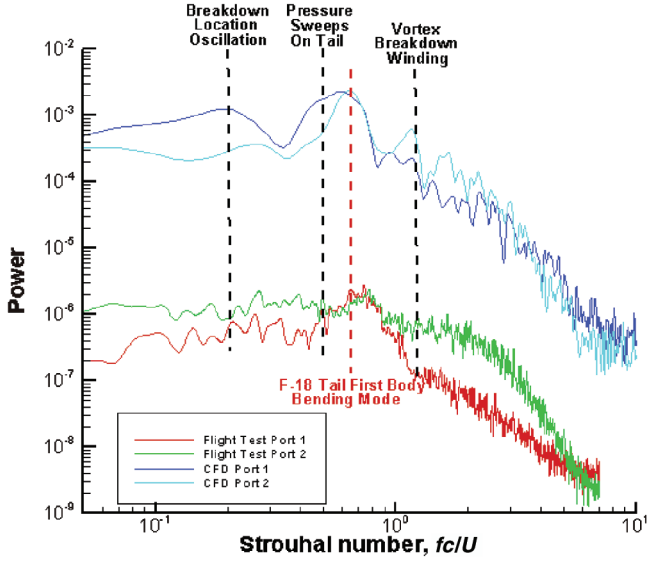

a)

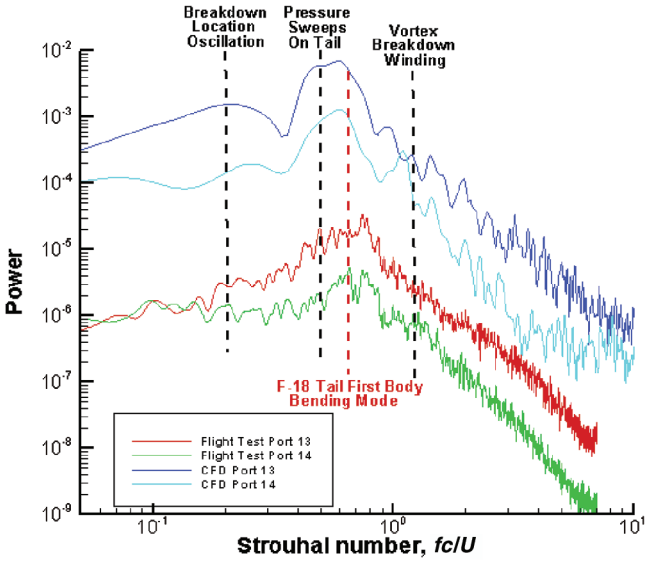

b)

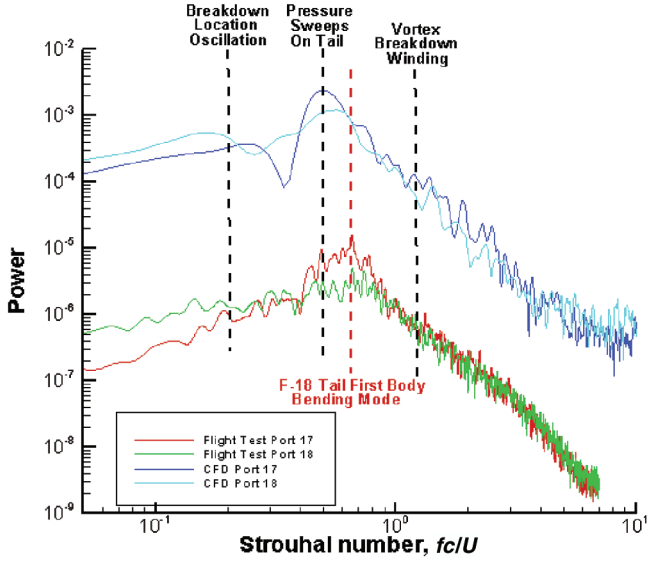

c)

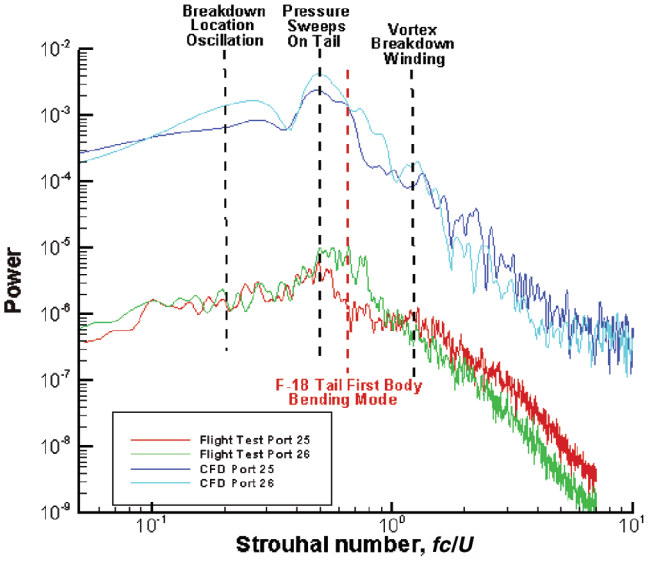

d)

Fig. 9 Comparison of power spectrum density from flight-test and DES prediction for ports a) 1–2, b) 13–14, c) 17–18, and d) 25–26.

and compute vortex breakdown locations either far upstream or downstream of the SADES method, as well as flight-test and experimentally obtained vortex breakdown positions. This mismatch in vortex breakdown mean position results in vastly different loads characteristics. In addition, the frequency content of tail pressures were more than three orders of magnitude lower in power than the corresponding SADES solutions, causing concern for their use in fluid–structure interaction simulations. The SADES solutions were then compared with flight-test Kulite pressures from the F-18 HARV vertical tails. The frequencies obtained with the SADES method matched the Kulite pressures remarkably well for both particular frequencies, and the overall character of the PSDs. This level of comparison shows the usefulness of this fluid-dynamics method for inclusion in a fluid–structure interaction method for these massively separated flow regimes.

Acknowledgments

The authors would like to thank Dave Fisher and Al Bowers of the NASA Dryden Flight Research Center for their invaluable assistance with the F-18 High Angle-of-Attack Research Vehicle flight-test data, as well as James Forsythe for modifying the F/A-18C grid during his U.S. Air Force Reserve duty. This work could not have been accomplished without the computational support of the Maui High Performance Computing Center of the High Performance Computing Management Office and the U.S. Air Force Academy Modeling and Simulation Research Center. Finally, the authors would like to express their gratitude for the support of this project by John Schmisseur of Air Force Office of Scientific Research.

References

[1] Lovell, D. A., "Military Vortices," *NATO RTO/AVT Symposium on Advanced Flow Management*, NATO RTO-MP-069, Paper KN-1, March 2003.

[2] Lee, B. H. K., "Vertical Tail Buffeting of Fighter Aircraft," *Progress in Aerospace Sciences*, Vol. 36, Nos. 3–4, 2000, pp. 193–279. doi:10.1016/S0376-0421(00)00003-8

[3] Fisher, D., Del Frate, J. H., and Zuniga, F. A., "Summary of In-Flight Flow Visualization Obtained From the NASA High Alpha Research Vehicle," NASA TM-101734, Jan. 1991.

[4] "High Alpha Research Vehicle Phase II Flight Report, Flight 197–199," NASA Ames Research Center, Dryden Flight Research Facility, HA94-70-660, Feb. 1994.

[5] Murman, S. M., Rizk, Y. M., Cummings, R. M., and Schiff, L. B., "Computational Investigation of Slot Blowing for Fuselage Forebody Flow Control," *Aircraft Design*, Vol. 2, No. 1, 1999, pp. 45–63. doi:10.1016/S1369-8869(99)00006-3

[6] Gee, K., Murman, S. M., and Schiff, L. B., "Computation of F/A-18 Tail Buffet," *Journal of Aircraft*, Vol. 33, No. 6, 1996, pp. 1181–1189.

[7] Morton, S. A., Steenman, M. B., Cummings, R. M., and Forsythe, J. R., "DES Grid Resolution Issues for Vortical Flows on a Delta Wing and an F-18C," AIAA Paper 2003-1103, Jan. 2003.

[8] Sheta, E. F., "Alleviation of Vertical Tail Buffeting of F/A-18 Aircraft," *Journal of Aircraft*, Vol. 41, No. 2, 2004, pp. 322–330.

[9] Spalart, P. R., and Allmaras, S. R., "A One Equation Turbulence Model for Aerodynamic Flows," *La Recherche Aerospatiale*, Vol. 1, 1994, pp. 5–21.

[10] Spalart, P., "Young-Person's Guide to Detached-Eddy Simulation Grids," NASA CR 2001-211032, 2001.

[11] Strang, W. Z., Tomaro, R. F., and Grismer, M. J., "The Defining Methods of Cobalt: A Parallel, Implicit, Unstructured Euler/Navier–Stokes Flow Solver," AIAA Paper 99-0786, Jan. 1999.

[12] Forsythe, J. R., Hoffmann, K. A., Cummings, R. M., and Squires, K. D., "Detached-Eddy Simulation with Compressibility Corrections Applied to a Supersonic Axisymmetric Base," *Journal of Fluids Engineering*, Vol. 124, No. 4, 2002, pp. 911–923. doi:10.1115/1.1517572

[13] Morton, S. A., Forsythe, J. R., Mitchell, A. M., and Hajek, D., "Detached-Eddy Simulations and Reynolds-Averaged Navier–Stokes Simulations of Delta Wing Vortical Flowfields," *Journal of Fluids Engineering*, Vol. 124, No. 4, 2002, pp. 924–932. doi:10.1115/1.1517570

[14] Squires, K. D., Forsythe, J. R., and Spalart, P. R., "Detached-Eddy Simulation of the Separated Flow Around a Forebody Cross-Section," *Direct and Large Eddy Simulation IV*, European Research Community on Flow, Turbulence and Combustion Series, Vol. 8, edited by B. J. Geurts, R. Friedrich, and O. Metais, Kluwar Academic, Norwell, MA, 2001, pp. 481–500.

[15] Forsythe, J. R., Squires, K. D., Wurtzler, K. E., and Spalart, P. R., "Detached-Eddy Simulation of the F-15E at High Alpha," *Journal of Aircraft*, Vol. 41, No. 2, 2004, pp. 193–200.

[16] Forsythe, J. R., and Woodson, S. H., "Unsteady CFD Calculations of Abrupt Wing Stall Using Detached-Eddy Simulation," AIAA Paper 2003-0594, Jan. 2003.

[17] Samareh, J., "Gridtool: A Surface Modeling and Grid Generation Tool," *Proceedings of the Workshop on Surface Modeling, Grid Generation, and Related Issues in CFD Solution*, NASA CP-3291, 1995.

[18] Pirzadeh, S., "Progress Toward a User-Oriented Unstructured Viscous Grid Generator," AIAA Paper 96-0031, Jan. 1996.

[19] Menter, F. R., "Improved Two-Equation k-ω Turbulence Models for Aerodynamic Flows," NASA TM-103975, 1992.

[20] Spalart, P. R., Jou W.-H., Strelets, M., and Allmaras, S. R., "Comments on the Feasibility of LES for Wings, and on a Hybrid RANS/LES Approach," *Advances in DNS/LES, First AFOSR International Conference on DNS/LES*, Greyden Press, Columbus, OH, Aug. 1997.

[21] Forsythe, J. R., Hoffmann, K. A., and Dieteker, F. F., "Detached-Eddy Simulation of a Supersonic Axisymmetric Base Flow with an Unstructured Flow Solver," AIAA Paper 2000-2410, June 2000.

[22] Morton, S. A., Forsythe, J. R., Squires, K. D., and Wurtzler, K. E., "Assessment of Unstructured Grids for Detached-Eddy Simulation of High Reynolds Number Separated Flows," *Proceedings of the 8th International Conference Numerical Grid Generation in Computational Field Simulations*, International Society for Grid Generation, Birmingham, AL, 2002, pp. 571–586.

[23] Mitchell, A. M., Morton, S. A., Forsythe, J. R., and Cummings, R. M., "Analysis of Delta-Wing Vortical Substructures Using Detached-Eddy Simulation," *AIAA Journal*, Vol. 44, No. 5, 2006, pp. 964–972.

[24] Pirzadeh, S. Z., "A Solution-Adaptive Unstructured Grid Method by Grid Subdivision and Local Remeshing," *Journal of Aircraft*, Vol. 37, No. 5, 2000, pp. 818–824.

[25] Morton, S. A., Forsythe, J. R., Mitchell, A. M., and Hajek, D., "DES and RANS Simulations of Delta Wing Vortical Flows," AIAA Paper 2002-0587, Jan. 2002.

[26] Ghaffari, F., "Navier–Stokes, Flight, and Wind Tunnel Flow Analysis for the F/A-18 Aircraft," NASA TP 3478, Dec. 1994.

[27] Gursul, I., "Review of Unsteady Vortex Flows over Delta Wings," AIAA Paper 2003-3942, June 2003.